Coastal Engineering 91 (2014) 191–199

Contents lists available at ScienceDirect

Coastal Engineering

journal homepage: www.elsevier.com/locate/coastaleng

Optimization of non-hydrostatic Euler model for water waves

Ling Zhu [a,b], Qin Chen [a,b,*], Xiaoliang Wan [b,c]

[a] Depart. of Civil and Environ. Eng., Louisiana State Univ., Baton Rouge, LA, USA
[b] Center for Computation and Tech., Louisiana State University, Baton Rouge, LA, USA
[c] Depart. of Mathematics, Louisiana State University, Baton Rouge, LA, USA

ARTICLE INFO

Article history:
Received 23 January 2014
Received in revised form 17 May 2014
Accepted 3 June 2014
Available online 6 July 2014

Keywords:
Euler equations
Sigma coordinate
Frequency dispersion
Optimal layer distribution
Fully dispersive
Nonlinear standing waves

ABSTRACT

The distribution of variables in the water column controls the dispersion properties of non-hydrostatic models. Because solving the Poisson equation is the most time consuming part of a non-hydrostatic model, it is highly desirable to reduce the number of unknowns in the water column by placing them at optimal locations. The paper presents the analytical dispersion relationship of a non-hydrostatic Euler model for water waves. The phase speed of linear waves simulated by the semi-discretized Euler model can be expressed as a rational polynomial function of the dimensionless water depth, kh, and the thicknesses of layers encompassing the water column become optimizable parameters in this function. The dispersion error is obtained by comparing this phase speed against the exact solution based on the linear wave theory. It is shown that for a given dispersion error (e.g. 1%), the range of kh can be extended if the layer thicknesses are optimally selected. The optimal two- and three-layer distributions for the aforementioned Euler model are provided. The Euler model with the optimized layer distribution shows good linear dispersion properties up to $kh \approx 9$ with two layers, and $kh \approx 49.5$ with three layers. The derived phase speed was tested against both numerical and exact solutions of standing waves for various cases. Excellent agreement was achieved. The model was also tested using the fifth-order Stokes theory for nonlinear standing waves. The phase speed of nonlinear waves follows a similar trend of the derived phase speed although it deviates proportionally with the increase of wave steepness ka_0. Thus, the optimal layer distribution can also be applied to nonlinear waves within a range of ka_0 and kh. The optimization method is applicable to other non-hydrostatic Euler models for water waves.

1. Introduction

In physical oceanography, and coastal and ocean engineering, an accurate and efficient prediction of surface waves is of paramount importance. In the past several decades with the rapid advances in computational technology, substantial efforts have been devoted to developing numerical models for simulating the propagation and evolution of water waves from deep water to the shoreline.

A widely used type of models is based on depth-averaged equations, such as Boussinesq-type models. The conventional Boussinesq models (e.g. Peregrine 1967) have the drawback of weak dispersion and weak nonlinearity, or a limited range of applicability. By introducing a reference velocity at an arbitrary vertical location as the velocity variable and choosing the location to match the Padé [2, 2] expansion of the exact linear dispersion relationship, Nwogu (1993) extended the applicability of the model to $kh \approx 3$, here k is the wave number, and h is the water depth. The dimensionless wave number kh serves as a dispersion criterion.

Many efforts have been put in to enhance the deep-water accuracy of the depth-integrated approach by developing high-order Boussinesq-type models. By utilizing a quartic polynomial approximation for the vertical profile of velocity field, Gobbi and Kirby (1999) developed a model with excellent linear dispersion properties up to $kh \approx 6$. The models of Madsen and Schäffer (1998), and Chen et al. (1998) also showed good linear dispersive wave properties up to $kh \approx 6$. Madsen et al. (2002) further improved the Boussinesq-type model and made it applicable to extremely deep-water waves with $kh \approx 40$. Agnon et al. (1999) presented a new procedure to achieve good nonlinear dispersion properties up to $kh \approx 6$.

Lynett and Liu (2004a and 2004b) introduced another approach to improving the dispersion accuracy of Boussinesq-type models. Instead of using a high-order approximation for the vertical profile of the flow field, they used N independent quadratic polynomial approximations for the velocity profiles. These polynomial approximations match at the interfaces that divide the water column into N layers. Good dispersion accuracy up to $kh \approx 8$ was achieved with an optimized two-layer model. Chazel et al. (2009) combined the approach in Madsen et al. (2002) and the approach in Lynett and Liu (2004a), and developed an

* Corresponding author. Tel.:+1 225 578 4911; fax: +1 225 578 4595.
E-mail address: qchen@lsu.edu (Q. Chen).

http://dx.doi.org/10.1016/j.coastaleng.2014.06.003
0378-3839/

efficient model with less complexity. This model exhibits good linear and nonlinear dispersion properties to $kh \approx 10$.

Another widely used type of models is based on the Navier–Stokes equations (NSE) or the Euler equations of fluid motion. The momentum equations are solved at every layer for this type of models, thus the computational cost is higher compared with the Boussinesq type models. To capture the rapid changing free surface and to apply the pressure boundary condition precisely on the free surface of the waves, Navier–Stokes models involve the non-hydrostatic pressure on the top layer, and solve this problem by methods of: (1) employing edged-based grid systems (e.g. Lin and Li, 2002; Zijlema and Stelling, 2005, 2008; Zijlema et al., 2011; Chen et al., 2011; Ma et al., 2012), (2) using the integration method (e.g. Yuan and Wu, 2004), (3) implementing interpolation approaches (e.g. Walters, 2005; Choi and Wu, 2006; Young et al., 2007), and (4) embedding Boussinesq-type like equation into the Navier–Stokes model (e.g. Wu et al., 2010).

To improve the model dispersion properties, non-uniform layers have been used. Finer vertical resolution is utilized near the free surface for capturing the rapid velocity and pressure variation while coarse resolution is used at the bottom due to the mild change of velocity and pressure in this region. Yuan and Wu (2006) presented a so-called top-down resolving (TDR) technique to determine a set of suitable thickness for layers. The basic concept of this technique is to keep a fine resolution from the top layers down to the one just above the bottom layer, and use a coarse resolution for the bottom layer. With this TDR method, their model can achieve the same dispersion accuracy using 5 non-uniform layers rather than using 10 uniform layers for waves with $kh = 4$.

Young and Wu (2009) provided the top-layer thickness for their two-layer non-hydrostatic model. For $kh = 3.14$, the top layer takes 50% of the water depth; for $kh = 6$, the top layer takes 39.3% of the water depth, and for $kh = 15$, the top layer takes 15.7% of the water depth. However, the dependence of the top layer thickness on kh values hinders the model application in resolving highly dispersive random waves. Young and Wu (2010) proposed an adapted top-layer control (ATLC) method that eliminates the model layer thickness dependence on kh. The basic concept is that the finer resolution of the top layer is given by $\Delta\sigma_N = 0.5 / (N - 1)$, where $\Delta\sigma_N$ is the top layer size, and N is the number of layers. The size of the rest layers exponentially stretches to the bottom layer. The top layer size is set as 50%, 25% and 12.5% for two-, three-, and five-layer models, respectively. For a given tolerance phase error of 1%, the two-, three-, and five-layer models are capable of resolving linear wave dispersion up to $kh = 3.14$, 6.28 and 15.7, respectively.

Zijlema and Stelling (2005, 2008) and Zijlema et al. (2011) proposed a non-hydrostatic, free-surface flow model, SWASH (an acronym of Simulating WAves till SHore) for simulating wave propagation from deep water to the surf zone, using a semi-implicit, staggered finite volume method. The adoption of the Keller-box scheme in this model enabled the pressure to be assigned at the free surface without any approximation, and also enabled good dispersion properties at very low vertical resolution (two or three layers). Using two uniform layers, for a 1% tolerance phase error, SWASH achieves good linear dispersion properties up to $kh \approx 7$ and 3 for standing waves and progressive waves, respectively. Using three uniform layers, for a 1% tolerance phase error, SWASH achieves good linear dispersion properties up to $kh \approx 7$ for progressive waves. Zijlema et al. (2011) suggested that adjusting layer thicknesses could significantly improve wave dispersion accuracy. With layer thickness tuned as 10%, 20%, and 70% of the total water depth, their three-layer model is able to simulate waves with $kh \approx 15.7$ with a relatively small phase error.

Bai and Cheung (2013) provide theoretical dispersion relationships for an N-layer Boussinesq-type system. The derived dispersion relationships follow a [2 N − 2, 2 N] Padé expansion. The accumulative dispersion error is computed over $0.01 \le kh \le 6$ for covering a wide spectrum of ocean waves from deep water to shoreline. The layer arrangement appears as free parameter and can be adjusted for minimizing the accumulative dispersion error, and optimizing the proposed model. The two-layer model with the optimal layer arrangement of 50%–50% of the water depth gives a minimum error of 3.445%. The three-layer model with the optimal layer arrangement of 29%–32%–39% of the water depth gives a minimum error of 3.09%.

Similar to Boussinesq-type models in which the location of the horizontal velocity in the water column controls the dispersion properties, the vertical distribution of the variables in non-hydrostatic free surface flow models dictates the model dispersion accuracy. Because solving the Poisson equation is the most time consuming part of a non-hydrostatic model, it is highly desirable to reduce the number of unknowns in the water column by placing them at optimal locations. The objective of our study is to derive the analytical dispersion relationship of a non-hydrostatic free surface flow model and optimize it for extremely dispersive and highly nonlinear waves with only two or three layers. Although the optimization method is applicable to all non-hydrostatic models, for the demonstration purpose, the present work chose a Euler model that uses the algorithm and numerical scheme presented in Zijlema and Stelling (2005), except using the finite difference method in a sigma-coordinate. In this paper, we will present: (1) the derivation of the phase speed of linear waves simulated by the semi-discretized non-hydrostatic Euler model, and (2) the optimal two- and three-layer distributions. For a 1% tolerance dispersion error, the optimal two-layer distribution from bottom to top is 67% and 33% of the total water depth and the Euler model is capable of simulating linear waves up to $kh = 9$. For a 1% tolerance dispersion error, the optimal three-layer distribution from bottom to top is 68%, 26.5% and 5.5% of the total water depth and the Euler model is capable of simulating extremely dispersive waves up to $kh = 49.5$.

Furthermore, nonlinear standing wave tests have been performed to examine the effect of nonlinearity. Kirby and Dalrymple (1986) proposed a nonlinear dispersion relation, which effectively approximated the dispersion characteristics of waves propagating from deep to shallow waters. The nonlinear effect was scaled by wave steepness ka_0, and the phase speed became a function of kh and ka_0. In this paper, numerical experiments with different ka_0 are conducted. A fifth-order Stokes-type exact solution for standing waves (Sobey, 2009) is utilized to test our model. We have found that the phase speed of nonlinear waves follows the analytically derived linear phase speed, although the discrepancy rises as ka_0 increases. Therefore the optimal layer distribution can also be applied to the nonlinear wave simulation.

This paper is organized as follows: Section 2 briefly describes the governing equations and the numerical schemes. Section 3 presents the numerical results in comparison with the exact solution to demonstrate the performance of the model. In Section 4, we derive the analytical dispersion relationship of this discretized system of Euler equations followed by the determination of the optimal two- and three-layer distributions for extremely dispersive waves. Section 5 is focused on the effect of wave nonlinearity on the model performance with the optimal layer distributions. Finally, Section 6 summarizes the findings and presents the conclusions.

2. The Euler model

2.1. Governing equations

The propagation of fully dispersive, nonlinear water waves is governed by the continuity equation and the incompressible Euler equations, which are written as

$$\frac{\partial u}{\partial x^*} + \frac{\partial w}{\partial z^*} = 0 \tag{1}$$

$$\frac{\partial u}{\partial t^*} + u\frac{\partial u}{\partial x^*} + w\frac{\partial u}{\partial z^*} + \frac{\partial p}{\partial x^*} = 0 \tag{2}$$

$$\frac{\partial w}{\partial t^*}+u\frac{\partial w}{\partial x^*}+w\frac{\partial w}{\partial z^*}+\frac{\partial p}{\partial z^*}=0 \tag{3}$$

where, (x^*,z^*) is the Cartesian coordinates, u and w are the velocity components in the x^*- and z^*-direction respectively, p is the total pressure. p is normalized by the water density ρ, and divided into hydrostatic part $g(\eta - z^*)$ and non-hydrostatic part q. Here, g is the gravitational acceleration, and η is the free surface elevation.

The physical computational domain is vertically bounded by the bottom $z^* = -h(x^*)$ and the free surface $z^* = \eta(x^*,t^*)$. To accurately represent the uneven bottom and the time dependent free surface, a σ-coordinate (Phillips, 1957) is adopted.

$$t = t^*, \quad x = x^*, \quad \sigma = \frac{z^*+h}{D} \tag{4}$$

where $D(x,t) = \eta(x,t) + h(x)$ is the total water depth. The mapped computational domain is a stationary rectangular area, with σ ranging from 0 to 1 corresponding to the bottom and the free surface, respectively. Based on the chain rule, the governing equations in the σ-coordinate (x, σ, t) take the forms

$$\frac{\partial u}{\partial x}+\frac{\partial u}{\partial \sigma}\frac{\partial \sigma}{\partial x^*}+\frac{\partial w}{\partial \sigma}\frac{\partial \sigma}{\partial z^*}=0 \tag{5}$$

$$\frac{\partial u}{\partial t}+u\frac{\partial u}{\partial x}+w_\sigma\frac{\partial u}{\partial \sigma}+g\frac{\partial \eta}{\partial x}+\frac{\partial q}{\partial x}+\frac{\partial q}{\partial \sigma}\frac{\partial \sigma}{\partial x^*}=0 \tag{6}$$

$$\frac{\partial w}{\partial t}+u\frac{\partial w}{\partial x}+w_\sigma\frac{\partial w}{\partial \sigma}+\frac{\partial q}{\partial \sigma}\frac{\partial \sigma}{\partial z^*}=0 \tag{7}$$

where, u and w are components of velocity in the x- and σ-direction, respectively, and

$$w_\sigma = \frac{D\sigma}{Dt^*}=\frac{\partial \sigma}{\partial t^*}+u\frac{\partial \sigma}{\partial x^*}+w\frac{\partial \sigma}{\partial z^*} \tag{8}$$

$$\frac{\partial \sigma}{\partial x^*}=\frac{1}{D}\frac{\partial h}{\partial x}-\frac{\sigma}{D}\frac{\partial D}{\partial x}, \quad \frac{\partial \sigma}{\partial z^*}=\frac{1}{D}, \quad \frac{\partial \sigma}{\partial t^*}=-\frac{\sigma}{D}\frac{\partial D}{\partial t}. \tag{9}$$

The kinematic boundary conditions at the free surface ($\sigma = 1$) and the impermeable bottom ($\sigma = 0$) are:

$$w|_{\sigma=1}=\frac{\partial \eta}{\partial t}+u\frac{\partial \eta}{\partial x} \tag{10}$$

$$w|_{\sigma=0}=-u\frac{\partial h}{\partial x}. \tag{11}$$

The dynamic boundary condition at the free surface ($\sigma = 1$) is zero atmospheric pressure

$$q|_{\sigma=1}=0. \tag{12}$$

The depth-integrated continuity equation can be obtained by integrating Eq. (1) through the water column. After applying the kinematic boundary conditions, the resulting equation in σ-coordinate reads

$$\frac{\partial \eta}{\partial t}+\frac{\partial}{\partial x}\left[D\int_0^1 u d\sigma\right]=0. \tag{13}$$

Waves are generated at the inflow boundary by prescribing the velocities and the surface elevation from the linear wave theory. At the outflow boundary, a sponge zone with a width of two wave lengths is enforced to eliminate the wave reflection from the boundary. Inside the sponge zone, the primitive variables are attenuated in the following manner:

$$\eta_j = \eta_j/C_s, \quad u_j = u_j/C_s, \quad w_j = w_j/C_s \tag{14}$$

in which C_s is the damping coefficient defined by

$$C_s = (\alpha_s)^{\gamma_s^{\,i}}, \quad i=0,\ldots,n \tag{15}$$

where α_s and γ_s are free parameters, and n is the number of grids in the sponge zone. Numerical tests showed that best elimination of reflected waves from the boundary is attained with $\alpha_s = 2$ and $\gamma_s = 0.88$ for short waves; whereas the so-called Sommerfeld radiation boundary condition needs to be utilized for long waves. Treatments of these two types of outflow boundary conditions can be found in Chen et al. (1999).

2.2. Numerical scheme and algorithm

The numerical method of this model follows the framework of SWASH (Zijlema and Stelling, 2005). The discretization of the governing equations is based on the Crank–Nicholson method, which gives second order accuracy in space and time. The adoption of the Keller-box scheme in this model enabled the pressure at the free surface to be assigned with the dynamic boundary condition without any approximation, and also enabled good dispersion properties at very low vertical resolution (two or three layers). The computational domain in σ-coordinate is divided into $NX \times NZ$ rectangular cells with width Δx and height $\Delta\sigma_k = \sigma_k - \sigma_{k-1}$, $k = 1, \ldots, NZ$. The grid points in x- and σ-direction are denoted as

$$\left\{X|x_{i+1/2} = i\Delta x, \quad i = 0,\ldots,NX\right\} \quad \text{and} \quad \{Z|\sigma_k = \sigma_{k-1} + \Delta\sigma_k, \quad k = 1,\ldots,NZ\}. \tag{16}$$

The velocity components are distributed in a staggered manner, (i.e. u and w are located at $(i + 1/2, k + 1/2)$ and (i,k), respectively). The non-hydrostatic pressure q is located at the same place as w in the Keller-box scheme. The free surface elevation, η, is defined at the center of the surface cell. Fig. 1 illustrates the layout of the all variables in the Keller-box scheme.

The algorithm can be decomposed into two phases to handle the hydrostatic and non-hydrostatic pressure separately. The employment of the pressure correction technique enables global mass conservation and local mass conservation. In the first phase (i.e. the hydrostatic phase), the hydrostatic part of the pressure, or the surface elevation (η), is computed. The horizontal moment equation (Eq. (6)) and the depth-integrated continuity equation (Eq. (13)) are discretized and coupled into a linear system of equations in $\Delta\eta$, which is the temporal

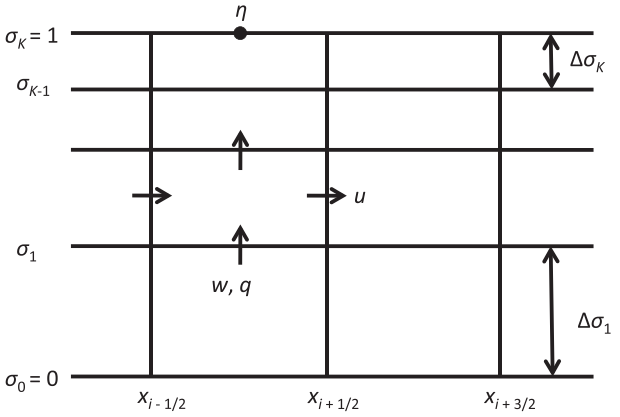

Fig. 1. The layout of the variables in the Keller-box scheme.

change in the surface elevation. In the second phase (i.e. the non-hydrostatic phase), the non-hydrostatic part of the pressure, q, is computed. The momentum equations (Eqs. (6) and (7)) and continuity equation (Eq. (5)) are discretized and coupled into the Poisson equation in Δq, which is the temporal change in the non-hydrostatic pressure. The Poisson equation is solved by the HYPRE (http://acts.nersc.gov/hypre), a software library for solving large-scale linear systems of equations on massively parallel computers. Jacobi and GMRES (Generalized Minimal RESidual) solvers are utilized to solve non-symmetric systems. Velocities u and w and pressure q are updated in this phase. More details about the numerical procedure can be found in Zijlema and Stelling (2005).

3. Model performance

The dispersion accuracy of the Euler model was examined through simulation of linear and non-linear dispersive waves. Tests results were compared with exact solutions from the linear wave theory. To study the capability of this model in resolving linear dispersion properties and nonlinear effect, three test cases are discussed in this section: (1) linear standing waves in a closed basin; (2) linear progressive waves in a flume; and (3) non-linear standing waves in a closed basin.

3.1. Linear standing waves

The numerical model was first tested against the exact solution of standing waves with an amplitude of $a_0 = 0.1$ m in a 20 m long closed basin. Dispersive waves ($kh = 2\pi$) were simulated to test the accuracy of this model. The computational domain contains 200 grids with uniform spacing of 0.1 m in the horizontal direction, and two layers with uniform thickness in the vertical direction. The time step Δt was set as $T/400$, where T is the wave period. Fig. 2 (upper panel) shows the comparison of the numerical and exact surface elevations at $x = 10$ m. The surface elevation was normalized by the wave amplitude a_0 and time was normalized by the wave period T. The computed surface elevations agree very well with the exact solution.

Define the relative dispersion error as $\Delta_e = |c_{model} - c_e|/c_e$. Fig. 3 shows that the relative dispersion error reduces as the number of the layers increases, and approaches a constant. For highly dispersive waves, more layers are required for achieving sufficiently accurate results. Finer vertical resolution can help improve the dispersion accuracy, but the computational cost goes up quickly as the vertical resolution of a non-hydrostatic Euler model increases. For this reason, in Section 4, we present a method to achieve high dispersion accuracy using a small number of layers (e.g. two or three layers).

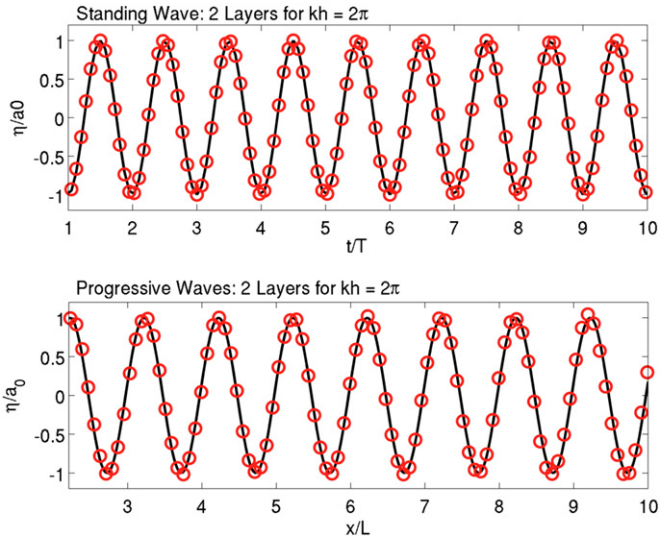

Fig. 2. Comparisons between the numerical (circles) and exact (solid line) surface elevations for standing waves (upper panel) and progressive waves (lower panel) with $kh = 2\pi$ using two uniform layers.

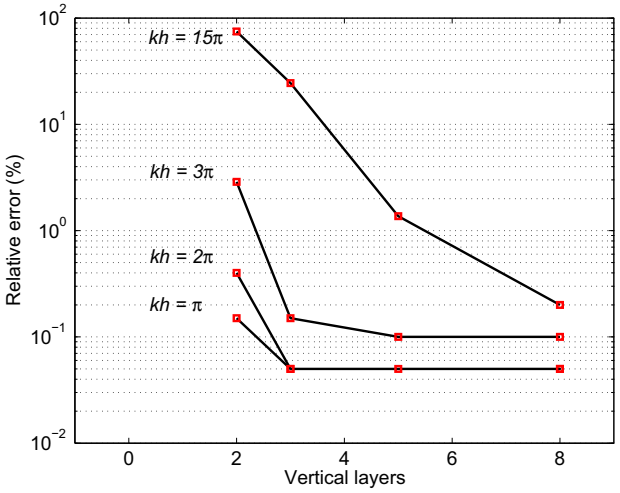

Fig. 3. Relative dispersion error at $x = 10$ m as a function of the number of layers and wave dispersion parameter kh.

3.2. Linear progressive waves on a flat bottom

The second test case is the linear progressive waves propagating in constant water depth. A wave train with an amplitude of $a_0 = 10^{-3}$ m and a wavelength of $L = 10$ m is generated at the left end of a 160 m long flume. The water depth is set as 10 m to make waves highly dispersive ($kh = 2\pi$). A 20 m long sponge zone is added at the right end of the flume to absorb the outgoing waves and minimize the reflection. The Courant number is defined as

$$Cr = \frac{\Delta t}{\Delta x}\left[\sqrt{gh} + max(u)\right]. \tag{17}$$

The computational domain used a uniform grid spacing of 0.2 m in the horizontal direction, and two layers with uniform thickness in the vertical direction. The time integration with respect to the convection terms is of explicit type. Thus, the Courant number was set as 0.1567, and the time step Δt was determined accordingly, which gives $\Delta t = T/800$, where T is the wave period. The high horizontal and temporal resolution minimizes the discretization errors in the x direction and time. Fig. 2 (lower panel) shows the comparisons of numerical and analytical surface elevations at $t = 80$ s. The surface elevation was normalized by the wave amplitude a_0 and time was normalized by the wave period T. The computed surface elevations agree well with the exact solution from the linear wave theory. The numerical result was taken one wave length from the left boundary to avoid small disturbances introduced by the inflow boundary.

4. Linear dispersion analysis

4.1. Linear dispersion properties for an N-layer model

In this section, the phase speed of linear waves simulated by the aforementioned non-hydrostatic Euler model is derived. The Keller-box scheme and the same layout of variables (i.e., velocities, pressure and surface elevation) are used in the derivation for the sake of consistency. The dispersion error is obtained by comparing this phase speed against the analytical phase speed from the linear wave theory.

The linearized governing equations in the Cartesian coordinate are written as follows:

$$\frac{\partial u}{\partial x}+\frac{\partial w}{\partial z}=0 \tag{18}$$

$$\frac{\partial u}{\partial t}+g\frac{\partial \eta}{\partial x}+\frac{\partial q}{\partial x}=0 \tag{19}$$

$$\frac{\partial w}{\partial t}+\frac{\partial q}{\partial z}=0 \tag{20}$$

$$\frac{\partial \eta}{\partial t}+\frac{\partial}{\partial x}\int_{-h}^{0} u dz=0. \tag{21}$$

The computational domain is divided into N layers. The layer thickness is denoted as $\Delta z_j = \alpha_j h (j = 1, 2, \ldots, N$, from the bottom layer to the top layer), where Δz_j is the thickness of layer j; h is the water depth; α_j is the ratio of thickness of layer j to the water depth. α_j satisfies the equality $\sum \alpha_j = 1$.

The derivation starts with the quasi-discrete vertical momentum equation, obtained by discretizing Eq. (20) in the vertical direction only.

$$\frac{1}{2}\left(\frac{\partial w_{j+1}}{\partial t}+\frac{\partial w_j}{\partial t}\right)+\frac{q_{j+1}-q_j}{\Delta z_{j+1}}=0, \quad j=0,\ldots,N-1 \tag{22}$$

The vertical momentum equation is discretized at the center of the layer, rather than at the interface of the layer. A flat bottom is considered here, thus $w_0 = 0$ and $\partial w_0/\partial t = 0$. The time derivative of vertical velocity is obtained from Eq. (22).

$$\frac{\partial w_1}{\partial t}=-2\frac{q_1-q_0}{\alpha_1 h} \tag{23}$$

$$\frac{\partial w_j}{\partial t}=-2\frac{q_j-q_{j-1}}{\alpha_j h}-\frac{\partial w_{j-1}}{\partial t}, \quad j=2,\ldots,N \tag{24}$$

By taking the temporal derivative of Eq. (18) and the spatial derivative of Eq. (19), and doing subtraction, we get

$$\frac{1}{\Delta z_j}\left(\frac{\partial w_j}{\partial t}-\frac{\partial w_{j-1}}{\partial t}\right)-g\frac{\partial^2 \eta}{\partial x^2}-\frac{1}{2}\left(\frac{\partial^2 q_j}{\partial x^2}+\frac{\partial^2 q_{j-1}}{\partial x^2}\right)=0, \quad j=1,\ldots,N. \tag{25}$$

The time derivative of vertical velocity from Eqs. (23) and (24), and the free surface dynamic boundary condition (i.e. $q_N = 0$) are substituted into Eq. (25), yielding

$$-2\frac{q_1-q_0}{\alpha_1^2 h^2}-g\frac{\partial^2 \eta}{\partial x^2}-\frac{1}{2}\left(\frac{\partial^2 q_1}{\partial x^2}+\frac{\partial^2 q_0}{\partial x^2}\right)=0 \tag{26}$$

$$-2\frac{q_j-q_{j-1}}{\alpha_j^2 h^2}-4\sum_{s=1}^{N-1}(-1)^s\frac{q_{j-s}-q_{j-s-1}}{\alpha_{j-s}\alpha_j h^2}-g\frac{\partial^2 \eta}{\partial x^2}-\frac{1}{2}\left(\frac{\partial^2 q_j}{\partial x^2}+\frac{\partial^2 q_{j-1}}{\partial x^2}\right)=0, \quad j=2,\ldots,N. \tag{27}$$

The pressure, the horizontal velocity and the surface elevation can be expressed in harmonic forms

$$q_j = Q_j e^{i\theta}, \quad u_j = U_j e^{i\theta}, \quad \eta = A e^{i\theta} \tag{28}$$

where $\theta = kx - \omega t$, k is the wave number, and ω is the angular frequency. According to the linear wave theory, the pressure can be further expressed as

$$q_j = m_j g A e^{i\theta}. \tag{29}$$

Substituting Eq. (29) into Eqs. (26) and (27) leads to a system of linear equations for m_j, which is

$$-2\frac{m_1-m_0}{\alpha_1^2}+(kh)^2+\frac{1}{2}(m_0+m_1)(kh)^2=0 \tag{30}$$

$$-2\frac{m_j-m_{j-1}}{\alpha_j^2}-4\sum_{s=1}^{k-1}(-1)^s\frac{m_{j-s}-m_{j-s-1}}{\alpha_{j-s}\alpha_j}+(kh)^2+\frac{1}{2}\left(m_j+m_{j-1}\right)(kh)^2=0, \quad j=2,\ldots,N. \tag{31}$$

By virtue of the Cramer's rule (Cramer, 1750), m_j can be expressed as a rational polynomial function of kh, with the maximum power equal to 2 N. The ratios of layer thicknesses to the water depth (α_j) play as free parameters in this function.

Applying the rectangle rule to Eq. (21) yields

$$\frac{\partial \eta}{\partial t}+\frac{\partial}{\partial x}\sum_{j=1}^{N} u_j \Delta z_j=0. \tag{32}$$

By substituting the expression of m_j, and harmonic forms of u, q and η into Eqs. (19) and (21), a system of linear equations for U_j and A is obtained:

$$-\omega A+kh\sum_{j=1}^{N}\alpha_j U_j=0 \tag{33}$$

$$\left[1+\frac{1}{2}\left(m_j+m_{j-1}\right)\right]gkA-\omega U_j=0, \quad j=1,\ldots,N. \tag{34}$$

In order to get a non-trivial solution for U_j and A, the determinant of the matrix must be equal to zero, which leads to the phase speed of linear waves simulated using this Euler model. The calculations were performed using MATHEMATICA.

4.2. Two-layer model

For a two layer model ($j = 2$), the pressure coefficients m_j can be expressed as:

$$m_0=\frac{-2(a_1-a_2+a_3)(kh)^2}{(kh)^4+(a_1-2a_2+a_3)(kh)^2+a_1 a_3} \tag{35}$$

$$m_1=\frac{-2(kh)^4-2(a_1-a_2)(kh)^2}{(kh)^4+(a_1-2a_2+a_3)(kh)^2+a_1 a_3} \tag{36}$$

$$m_2=0 \tag{37}$$

where $a_1 = 4/\alpha_1^2$, $a_2 = -8/\alpha_1\alpha_2$, $a_3 = 4/\alpha_2^2$. The dispersion relationship for the two-layer model is expressed as

$$\omega^2=gk\left[kh\left(1+\frac{1}{2}\alpha_1(m_0+m_1)+\frac{1}{2}\alpha_2 m_1\right)\right]. \tag{38}$$

The phase speed c_{model} becomes

$$c_{model} = (gh)^{1/2}\left[kh\left(1+\frac{1}{2}\alpha_1(m_0+m_1)+\frac{1}{2}\alpha_2 m_1\right)\right]^{1/2}. \quad (39)$$

The dispersion error is obtained by comparing this phase speed against the analytical phase speed, c_e, from the linear wave theory. The relative dispersion error $\Delta_e = |c_{model} - c_e|/c_e$ is obtained as

$$\Delta_e = \left[\frac{kh}{tanh(kh)}\left(1+\frac{1}{2}\alpha_1(m_0+m_1)+\frac{1}{2}\alpha_2 m_1\right)\right]^{1/2} - 1. \quad (40)$$

For a 1% tolerance dispersion error, the two-equidistant-layer model can simulate waves with kh up to 7. This dispersion accuracy is consistent with that of SWASH. A simple loop algorithm is utilized to find out the optimal layer thickness. Since α_1 plays as the only free parameter in the dispersion error expression for the two-layer model, we started at $\alpha_1 = 0.01$ (1% of water depth h) with increment of 0.001 and select the optimal 1 to maximize the range of kh for a given tolerance dispersion error. A summary of the optimization results is shown in Table 1. For simulating waves with a fixed kh value, Eq. (40) can be utilized to determine an appropriate layer distribution for achieving the minimum dispersion error.

To examine the model's dispersion properties, a series of numerical tests, both standing wave tests and progressive wave tests, were conducted. The phase errors were quantified and compared with the theoretically derived results (i.e. Eq. (40)). Excellent agreement has been obtained although small discrepancies between numerical and analytical phase speeds were observed for progressive wave test cases because of the inflow and outflow boundary effect. In the following parts of this paper, only standing wave test results are discussed. The wavelength L is fixed as 20 m, and the water depth h varies. The wave amplitude a_0 is set as 10^{-4} m to eliminate nonlinear effects.

Fig. 4 shows the comparison of the relative phase errors obtained theoretically and numerically using equidistant (upper panel) and optimal (lower panel) layer distributions with a 1% tolerance dispersion error. The numerical results exhibit excellent agreement with the theoretical estimates, which indicates that the derived phase speed accurately represents the linear dispersion properties of this model. Fig. 5 shows the theoretical and numerical phase speeds with the optimal layer distribution. The wave speeds were normalized by the exact solution from the linear wave theory. As seen in the inset, the simulated free surface elevations are in good agreement with the exact solution for $kh = 9.08$.

4.3. Three-layer model

For a three-layer model ($j = 3$), the pressure coefficient m_j can be expressed as:

$$m_0 = \frac{B_1^0(kh)^2 + B_2^0(kh)^4 + B_3^0(kh)^6}{C_0 + C_1(kh)^2 + C_2(kh)^4 + C_3(kh)^6} \quad (41)$$

$$m_1 = \frac{B_1^1(kh)^2 + B_2^1(kh)^4}{C_0 + C_1(kh)^2 + C_2(kh)^4 + C_3(kh)^6} \quad (42)$$

Table 1
Optimal layer distribution for the two-layer model.

Tolerance dispersion error (%)	Upper limit of kh range	Layer distribution (percentage of the water depth) from bottom to top
0.1	0.32	51%–49%
0.5	0.86	50%–50%
1	9.08	67%–33%

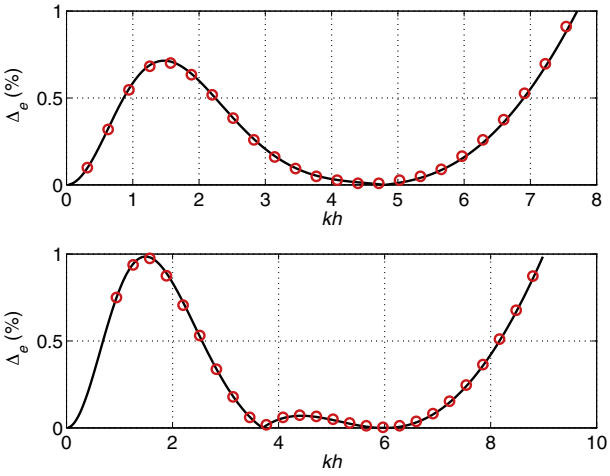

Fig. 4. Comparison of the relative phase errors obtained theoretically (solid lines) and numerically (circles) using two equally distributed (upper panel) and optimally distributed (lower panel) layers bounded by a 1% tolerance dispersion error.

$$m_2 = \frac{B_1^2(kh)^2 + B_2^2(kh)^4 + B_3^2(kh)^6}{C_0 + C_1(kh)^2 + C_2(kh)^4 + C_3(kh)^6} \quad (43)$$

$$m_3 = 0 \quad (44)$$

where the coefficients B_1^0, B_2^0, B_1^1, B_2^1, B_1^2, B_2^2, B_3^2, C_0, C_1, C_2 and C_3 are given in Appendix A. The dispersion relationship for the three-layer model is expressed as

$$\omega^2 = gk\left[kh\left(1+\frac{1}{2}\alpha_1(m_0+m_1)+\frac{1}{2}\alpha_2(m_1+m_2)+\frac{1}{2}\alpha_3 m_2\right)\right]. \quad (45)$$

The phase speed c_{model} becomes

$$c_{model} = (gh)^{1/2}\left[1+\frac{1}{2}\alpha_1(m_0+m_1)+\frac{1}{2}\alpha_2(m_1+m_2)+\frac{1}{2}\alpha_3 m_2\right]^{1/2}. \quad (46)$$

The dispersion error Δ_e is obtained as

$$\Delta_e = \left[\frac{kh}{tanh(kh)}\left(1+\frac{1}{2}\alpha_1(m_0+m_1)+\frac{1}{2}\alpha_2(m_1+m_2)+\frac{1}{2}\alpha_3 m_2\right)\right]^{1/2} - 1. \quad (47)$$

For a 1% tolerance dispersion error, the three-equidistant-layer model can simulate waves with kh up to 16.4. Two variables α_1 and α_2 play as free parameters in the selection of the optimal layer thicknesses. A summary of the optimization results is shown in Table 2.

Fig. 6 shows the comparison of the relative phase errors obtained theoretically and numerically using equidistant (upper panel) and optimal (lower panel) layer distributions bounded by a 1% tolerance dispersion error. The numerical results exhibit excellent agreement with the theoretical estimates. Fig. 7 shows the theoretical and numerical phase speeds with the optimal layer distribution. The wave speeds were normalized by the exact solution from the linear wave theory. As seen in the inset, the simulated free surface elevations are in good agreement with the exact solution for $kh = 49.5$.

For the three-layer model, the highest polynomial order of kh in the numerator and denominator in the expression of phase speed reaches 6, compared with 4 for the two-layer model. This explains why the three-layer model can produce more accurate results than the two-layer model. The dispersion accuracy is drastically improved by increasing

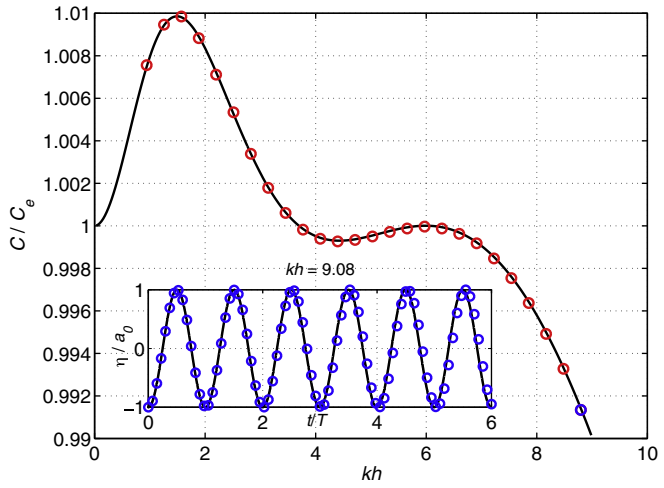

Fig. 5. Comparison of the theoretically derived (solid line) and numerically obtained (circles) phase speeds with two optimally distributed layers. Inset: comparison of numerical (circles) and exact (solid line) solutions of surface elevations for $kh = 9.08$.

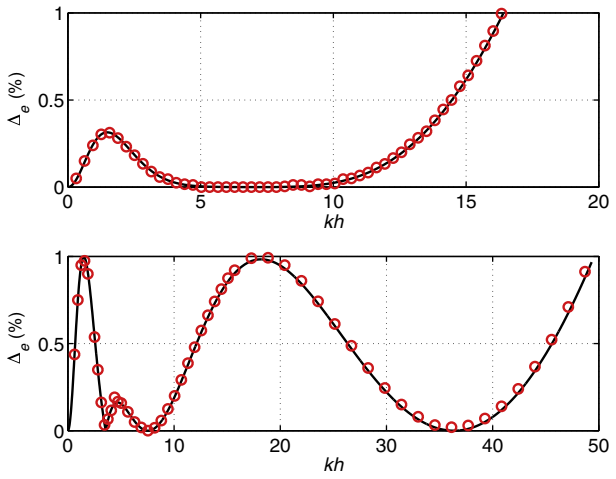

Fig. 6. Comparison of the relative phase errors obtained theoretically (solid lines) and numerically (circles) using three equally distributed (upper panel) and optimally distributed (lower panel) layers bounded by a 1% tolerance dispersion error.

the number of layers or by using optimal layer distribution as shown in Fig. 8.

5. Evaluation of the nonlinear effect

5.1. Nonlinearity parameter

The aforementioned dispersion relationships were derived assuming wave steepness ka (where a is the characteristic wave amplitude) was infinitely small, or $ka \ll 1$. However, for large amplitude waves, the wave properties and analytical dispersion relationship involve a power series of ka (e.g. Sobey, 2009); therefore, the nonlinearity can be scaled by the wave steepness ka. The breaking criterion limits the maximum amplitude of wave to be $2a/L \approx 0.14$ ($ka \approx 0.44$) in deep water (Longuet-Higgins, 1973; Michell, 1893). The derivation of dispersion relationship for nonlinear waves is not trivial due to nonlinear terms in the governing equations. However we can attain the dispersion curves numerically.

Nonlinear standing waves with an amplitude a_0 sloshing in a 20 m long closed basin were simulated to examine the performance of this Euler model in simulating nonlinear dispersive waves. Exact solutions, based on a fifth-order Stokes theory (Sobey, 2009), were used to specify the initial conditions and verify the model results. The non-linear dispersion relationship derived by Sobey (2009) reads

$$(gk)^{1/2}\sum_{i=1}^{5}(ka_0)^{(i-1)}D_i = 2\pi/T \tag{48}$$

where D_i are dimensionless coefficients given in Appendix B. The phase speed, affected by the wave nonlinearity, becomes a function of kh and ka_0. The three-layer model using the optimal vertical layout was utilized to predict waves with four wave steepnesses, ranging from linear ($ka_0 = 0.000314$), weakly nonlinear ($ka_0 = 0.157$), and strongly nonlinear ($ka_0 = 0.314$) to the wave breaking limit ($ka_0 = 0.44$). Also, for a given tolerance dispersion error (1%), the maximum kh is found for ka_0 ranging from 0.000314 to 0.44 with an increment of 0.05.

Table 2
Optimal layer distribution for the three-layer model.

Tolerance dispersion error (%)	Upper limit of kh range	Layer distribution (percentage of the water depth) from bottom to top
0.1	0.5	33.4%–33.3%–33.3%
0.5	23.5	45%–43%–12%
1	49.5	68%–26.5%–5.5%

5.2. Numerical results

Fig. 9 shows the comparison of the relative phase speeds (c/c_e) obtained theoretically (linear) and numerically (nonlinear) for the four types of waves. For nonlinear waves the phase speed follows a similar trend to the derived phase speed for linear waves but deviates proportionally with the increase of ka_0; therefore, the optimal layer distribution based on the linear dispersion relationship of the discretized Euler equations can also be utilized to simulate nonlinear waves within a range of ka_0 and kh. Table 3 lists the maximum kh for different ka_0 with the dispersion error limited to 1%. In practical applications, if ka_0 is known, a rough range of kh can be estimated and within this range the optimized model can provide numerical results with a dispersion error less than 1%.

Fig. 10 shows the comparison of the modeled surface elevation and fifth-order Stokes solution (Sobey, 2009) under four types of wave conditions corresponding to the maximum kh values of 49.50, 11.95, and 2.83, respectively. It is seen that the numerical model with the

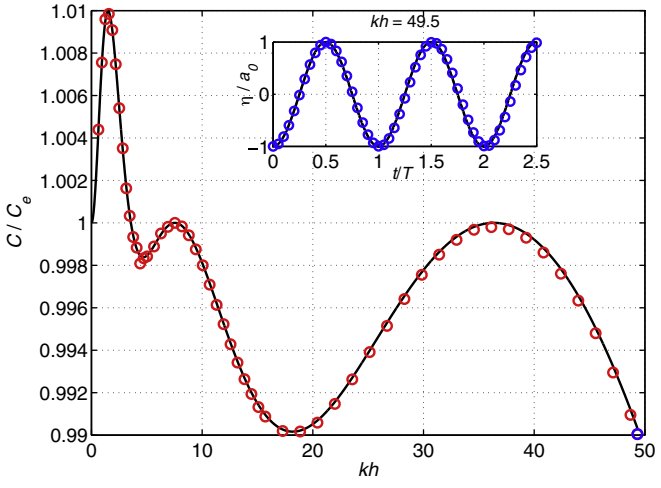

Fig. 7. Comparison of the theoretically derived (solid line) and numerically obtained (circles) phase speeds with three optimally distributed layers. Inset: comparison of numerical (circles) and exact (solid line) solutions of surface elevations for $kh = 49.5$.

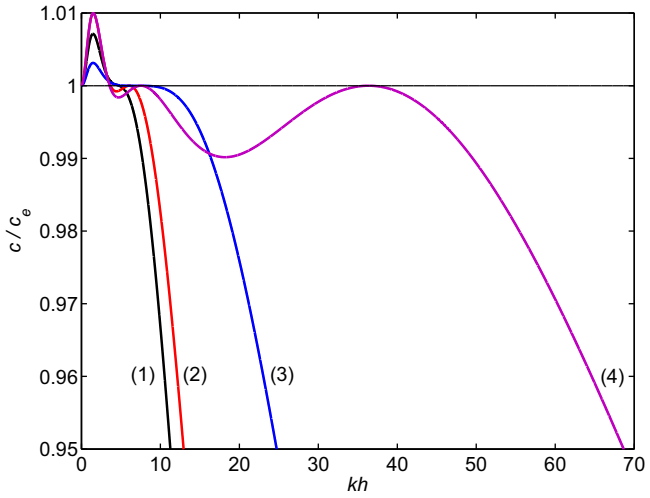

Fig. 8. Comparison of relative phase speeds for the two-layer and three-layer models using equidistant and optimal layer distributions. Curve (1): Two layers with constant layer thickness; (2) two layers with optimal layer distribution; (3): three layers with constant layer thickness; (4): three layers with optimal layer distribution.

optimized layer thickness captures the wave nonlinearity quite well in comparison with the Stokes solutions of nonlinear stranding waves.

6. Conclusions

A model for simulating the propagation of fully dispersive, nonlinear water waves was developed following the Keller-box scheme and the numerical algorithm presented in the SWASH model. The aim of this paper was to develop a theoretically sound method to optimize non-hydrostatic Euler models for extremely dispersive, nonlinear water waves. The key findings are as follows:

1. The theoretical phase speed of linear waves simulated by the non-hydrostatic Euler model is provided in this paper. It is a rational polynomial function of the dimensionless water depth, kh, and the thicknesses of layers encompassing the water column appear as free parameters in this function. The dispersion error thereupon is obtained by comparing this phase speed against the exact solution from the linear wave theory.

Table 3
The maximum kh for different ka_0 with 1% dispersion error.

ka_0	Maximum kh
0.000314–0.16	49.50
0.2	13.82
0.25	12.57
0.314	11.94
0.35	4.40
0.4	3.45
0.44	2.83

2. For a 1% tolerance dispersion error, the optimal layer distribution of a two-layer model from bottom to top is 67% and 33% of the water depth, and with this optimal layer distribution the model can simulate waves up to $kh = 9.08$.
3. For a 1% tolerance dispersion error, the optimal layer distribution of a three-layer model from bottom to top is 68%, 26.5% and 5.5% of the water depth, and with this optimal layer distribution the model can simulate waves up to $kh = 49.5$.
4. The phase speed of simulated nonlinear waves follows a trend similar to linear waves; therefore, the optimal layer distribution can be applied to nonlinear wave simulations as well. A table is provided for estimating the applicable range of kh for a given ka_0 to simulate nonlinear waves with less than a 1% dispersion error.
5. It has been shown that the derived dispersion relationships for two- and three-layer models are valid. Such a technique can be extended to any number of layers. Moreover, the methodology can be applied to other non-hydrostatic models for water waves to minimize the number of layers needed to simulate a wide spectrum of ocean waves from deep to shallow waters.

Acknowledgments

The study was supported by the US National Science Foundation (NSF) (CBET-0652859 and DMS-1115527). Any opinions, findings and conclusions or recommendations expressed in this paper are those of the authors and do not necessarily reflect the views of the NSF.

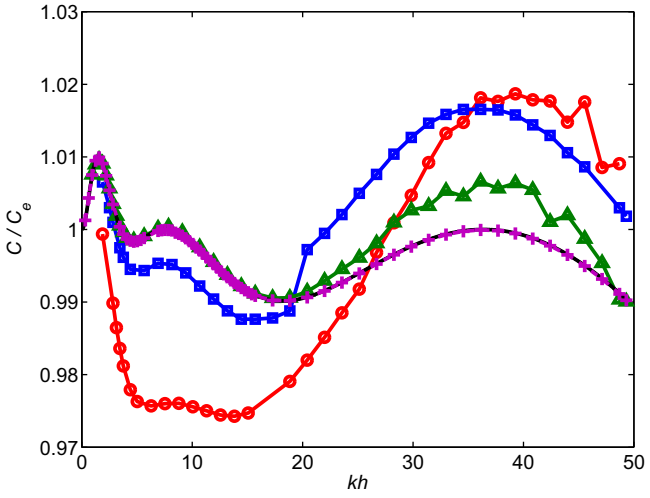

Fig. 9. Comparison of relative phase speeds obtained from theoretical derivation (black solid line) and numerical experiments for linear waves ($ka_0 = 3e-4$, cross), weakly nonlinear waves ($ka_0 = 0.157$, triangle), strongly nonlinear waves ($ka_0 = 0.314$, square), and extremely nonlinear waves ($ka_0 = 0.440$, circle).

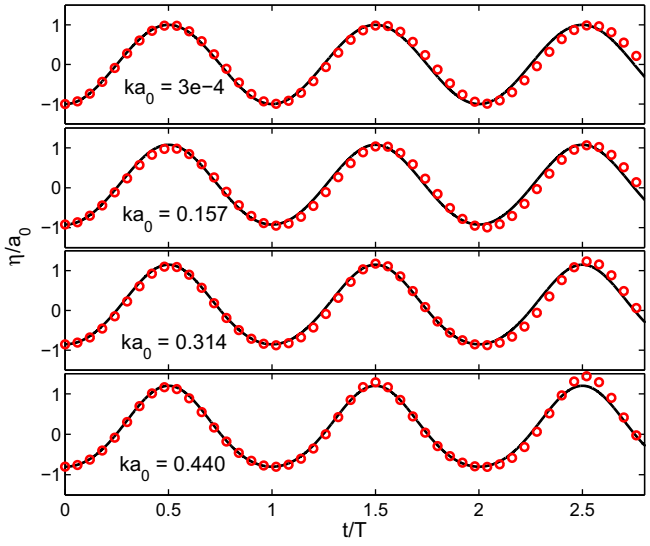

Fig. 10. Comparison of numerical (circles) and fifth-order Stokes (solid line) solutions of surface elevations for linear waves ($ka_0 = 3e-4$, and $kh = 49.50$), weakly nonlinear waves ($ka_0 = 0.157$, and $kh = 49.50$), strongly nonlinear waves ($ka_0 = 0.314$, and $kh = 11.94$), and extremely nonlinear waves ($ka_0 = 0.440$, and $kh = 2.83$).

Appendix A. Dispersion relation coefficients for the three-layer model

The coefficients B_1^0, B_2^0, B_1^1, B_2^1, B_1^2, B_2^2, B_3^2, C_0, C_1, C_2 and C_3 for the three-layer model are given as

$$B_1^0 = -4\alpha_1^2 - 4\alpha_2^2 - 4\alpha_3^2 - 8\alpha_1\alpha_2 - 8\alpha_1\alpha_3 - 8\alpha_2\alpha_3 \tag{A.1}$$

$$B_2^0 = -2\alpha_1^2\alpha_2\alpha_3 - 2\alpha_1\alpha_2^2\alpha_3 - 2\alpha_3^2\alpha_1\alpha_2 \tag{A.2}$$

$$B_3^0 = -\frac{1}{4}\alpha_1^2\alpha_2^2\alpha_3^2 \tag{A.3}$$

$$B_1^1 = -8\alpha_1\alpha_2 - 8\alpha_1\alpha_3 - 8\alpha_2\alpha_3 - 4\alpha_2^2 - 4\alpha_3^2 \tag{A.4}$$

$$B_2^1 = -\alpha_1^2\alpha_2^2 - \alpha_1^2\alpha_3^2 - 2\alpha_1^2\alpha_2\alpha_3 - 2\alpha_1\alpha_2^2\alpha_3 - 2\alpha_1\alpha_2\alpha_3^2 \tag{A.5}$$

$$B_1^2 = -8\alpha_1\alpha_3 - 8\alpha_2\alpha_3 - 4\alpha_3^2 \tag{A.6}$$

$$B_2^2 = -2\alpha_1^2\alpha_2\alpha_3 - 2\alpha_1\alpha_2^2\alpha_3 - \alpha_1^2\alpha_3^2 - 4\alpha_1\alpha_2\alpha_3^2 - \alpha_2^2\alpha_3^2 \tag{A.7}$$

$$B_3^2 = -\frac{1}{4}\alpha_1^2\alpha_2^2\alpha_3^2 \tag{A.8}$$

$$C_0 = 8 \tag{A.9}$$

$$C_1 = 2\alpha_1^2 + 2\alpha_2^2 + 2\alpha_3^2 + 8\alpha_1\alpha_2 + 8\alpha_1\alpha_3 + 8\alpha_2\alpha_3 \tag{A.10}$$

$$C_2 = \frac{1}{2}\alpha_1^2\alpha_2^2 + \frac{1}{2}\alpha_1^2\alpha_3^2 + \frac{1}{2}\alpha_2^2\alpha_3^2 + 2\alpha_1^2\alpha_2\alpha_3 + 2\alpha_1\alpha_2^2\alpha_3 + 2\alpha_1\alpha_2\alpha_3^2 \tag{A.11}$$

$$C_3 = \frac{1}{8}\alpha_1^2\alpha_2^2\alpha_3^2. \tag{A.12}$$

Appendix B. Dimensionless coefficients of dispersion relationship for stokes waves

Let $q = \tanh(kh)$, the dimensionless coefficients D_i are given as (Sobey, 2009)

$$D_1 = q^{1/2} \tag{B.1}$$

$$D_2 = 0 \tag{B.2}$$

$$D_3 = -\frac{1}{64}\frac{-9 + 3q^4 + 12q^2 + 2q^6}{q^{7/2}} \tag{B.3}$$

$$D_4 = 0 \tag{B.4}$$

$$D_5 = -\frac{1}{16384}\frac{12q^{16} - 176q^{14} - 681q^{12} + 201q^{10} + 279q^8 - 978q^6 - 279q^4 + 513q^2 + 405}{q^{19/2}}. \tag{B.5}$$

References

Agnon, Y., Madsen, P.A., Schäffer, H., 1999. A new approach to high order Boussinesq models. J. Fluid Mech. 399, 319–333.

Bai, Y., Cheung, K.F., 2013. Dispersion and nonlinearity of multi-layer non-hydrostatic free-surface flow. J. Fluid Mech. 726, 226.

Chazel, F., Benoit, M., Ern, A., Piperno, S., 2009. A double-layer Boussinesq-type model for highly nonlinear and dispersive waves. R. Soc. Lond. A 465, 2319–2346.

Chen, Q., Madsen, P.A., Schäffer, H.A., Basco, D.R., 1998. Wave–current interaction based on an enhanced Boussinesq approach. Coast. Eng. 33, 11–39.

Chen, Q., Madsen, P.A., Basco, D.R., 1999. Current effects on nonlinear interactions of shallow-water waves. J. Waterw. Port Coast. Ocean Eng. 125 (4), 176186.

Chen, Q., Fan, Q., Ko, S.H., Huang, H., Allen, G., 2011. An Euler solver for nonlinear water waves using a modified staggered grid and Gaussian quadrature approach. Proceedings of the Sixth International Conference on Fluid Mechanics, June 30-July 3, 2011, Guangzhou, China.

Choi, D.Y., Wu, C.H., 2006. A new efficient 3D non-hydrostatic free-surface flow model for simulating water wave motions. Ocean Engineering 33 (5–6), 587–609.

Cramer, G., 1750. Intr. à l'analyse de lignes courbes algébriques (in French). pp. 657–659 (Geneva).

Gobbi, M.F., Kirby, J.T., 1999. Wave evolution over submerged sills: tests of a high-order Boussinesq model. Coast. Eng. 37, 57–96.

HYPRE, 2013. http://acts.nersc.gov/hypre/ [accessed: Jan. 3, 2014].

Kirby, J.T., Dalrymple, R.A., 1986. An approximate model for nonlinear dispersion in monochromatic wave propagation models. Coastal Engineering 9, 545–561.

Lin, P., Li, C.W., 2002. A sigma-coordinate three-dimensional numerical model for surface wave propagation. Int. J. Numer. Methods Fluids 38, 1045–1068.

Longuet-Higgins, M.S., 1973. On the form of the highest progressive and standing waves in deep water. Proc. R. Soc. Lond. A331, 445–456.

Lynett, P., Liu, P.L.-F., 2004a. A two-layer approach to wave modeling. R. Soc. Lond. A8, 2637–2669.

Lynett, P., Liu, P.L.-F., 2004b. Linear analysis of the multi-layer model. Coast. Eng. 51, 439–454.

Ma, G., Shi, F., Kirby, J.T., 2012. Shock-capturing non-hydrostatic model for fully dispersive surface wave processes. Ocean Model. 4344, 2235.

Madsen, P.A., Schäffer, H.A., 1998. Higher order Boussinesq-type equations for surface gravity waves-derivation and analysis. R. Soc. Lond. A 356, 1–60.

Madsen, P.A., Bingham, H.B., Liu, H., 2002. A new Boussinesq method for fully nonlinear waves from shallow to deep water. J. Fluid Mech. 462, 1–30.

Michell, J.H., 1893. The highest waves in water. Phil. Mag. Lond. 36, 430–437.

Nwogu, O., 1993. Alternative form of Boussinesq equations for nearshore wave propagation. J. Waterw. Port Coast. Ocean Eng. 119 (6), 618–638.

Peregrine, D.H., 1967. Long waves on a beach. J. Fluid Mech. 27, 815–827.

Phillips, N.A., 1957. A coordinate system having some special advantages for numerical forecasting. J. Meteorol. 14, 184–185.

Sobey, R.J., 2009. Analytical solutions for steep standing waves. Proceedings of the Institution of Civil Engineers Engineering and, Computational Mechanics. 162, p. 185197 (December, 2009. EM4).

Walters, R.A., 2005. A semi-implicit finite element model for non-hydrostatic (dispersive) surface waves. Int. J. Numer. Methods Fluids 49, 721–737.

Wu, C.H., Young, C.-C., Chen, Q., Lynett, P., 2010. Efficient nonhydrostatic modeling of surface waves from deep to shallow water. J. Waterw. Port Coast. Ocean Eng. 136 (2), 104–118.

Young, C.C., Wu, C.H., Kuo, J.T., Liu, W.C., 2007. A higher-order sigma-coordinate non-hydrostatic model for nonlinear surface waves. Ocean Engineering 34 (10), 1357–1370.

Young, C.C. And, Wu, C.H., 2009. An efficient and accurate non-hydrostatic model with embedded Boussinesq-type like equations for surface wave modeling. Int. J. Numer. Methods Fluids 60 (1), 27–53.

Young, C.-C., Wu, C.H., 2010. A σ-coordinate non-hydrostatic model with embedded Boussinesq-type like equations for modeling deep-water waves. Int. J. Numer. Methods Fluids 63, 1448–1470.

Yuan, H., Wu, C.H., 2004. A two-dimensional vertical non-hydrostatic model with an implicit method for free-surface flows. Int. J. Numer. Methods Fluids 44, 811–835.

Yuan, H., Wu, C.H., 2006. Fully nonhydrostatic modeling of surface waves. J. Eng. Mech. 132, 447–456.

Zijlema, M., Stelling, G.S., 2005. Further experiences with computing non-hydrostatic free-surface flows involving water waves. Int. J. Numer. Methods Fluids 48, 169–197.

Zijlema, M., Stelling, G.S., 2008. Efficient computation of surf zone waves using the nonlinear shallow water equations with non-hydrostatic pressure. Coast. Eng. 55, 780–790.

Zijlema, M., Stelling, G.S., Smit, P., 2011. SWASH: an operational public domain code for simulating wave fields and rapidly varied flows in coastal waters. Coast. Eng. 58, 992–1012.